Quantitative retinal imaging with optical coherence tomography

Gräfe, M.G.O.

2020

document version
Publisher's PDF, also known as Version of record

Chapter 3 |

Polarization-sensitive OCT

3.1 Birefringence

In polarization sensitive OCT not just the amplitude and phase of the electrical field of the light is recorded but also changes to the polarization state by the sample. The polarization state of the light can be affected by a medium if its optical properties depend on the polarization state itself. This effect is called birefringence [1]. It can be divided into intrinsic birefringence and form birefringence (also structural birefringence). Intrinsic birefringence occurs in specific crystals due to their crystalline structure. For birefringent structures in the human body, form birefringence is more important because it is caused by fibrous tissue. The anisotropic geometry of fibers causes the refractive index to be polarization dependent [1, 2]. Examples of the propagation of two orthogonally polarized light waves (electric field) in an isotropic and a birefringent medium are shown in Fig. 3.1. The refractive index determines the velocity of light in a medium $c = c_0/n$. In the isotropic medium the refractive index is independent of the polarization of the light. In the birefringent medium the refractive index is dependent on the polarization. This causes light of different polarizations to propagate with different velocities through the medium and one accumulates a phase delay η in comparison to the other one after passing a distance Δz through the birefringent medium. Throughout this thesis, this phase delay is called cumulative phase retardation. It can be expressed with Δn the difference of the refractive indexes and λ_V the vacuum wavelength [1]

$$\eta = \frac{2\pi\Delta z \cdot \Delta n}{\lambda_V}. \tag{3.1}$$

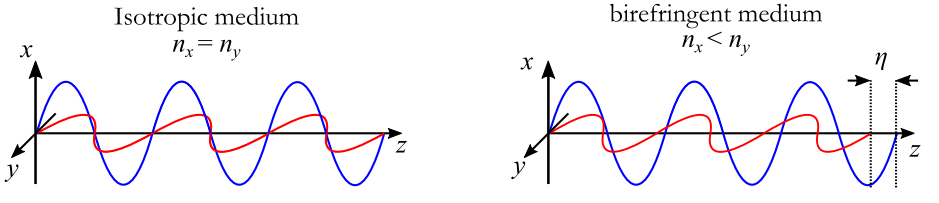

Fig. 3.1. Effect of birefringence on two orthogonal polarizations. In an isotropic medium the refractive index is independent of the polarization plane. In a birefringent medium the refractive index varies based on the polarization state of the light and with it the propagation speed. This leads to a phase retardation η between electromagnetic waves of two different polarization states.

Another important parameter for the characterization and imaging of birefringence in a biological sample is the optic axis orientation. For every birefringent medium a propagation direction can be found for which the refractive index is independent of the polarization direction. The axis of this propagation direction is called optic axis [3].

3.2 Mathematical formalisms

Two formalisms are used to describe birefringence and the interaction of light with birefringent media: Jones-calculus and Mueller-Stokes-calculus. Both are described in this section.

3.2.1 Jones-calculus

In the Jones-calculus the polarization state of the light is described by a two-component complex-valued vector where the two components are assigned to orthogonal polarization states [4]

$$\mathbf{E} = \begin{pmatrix} E_{\parallel} \\ E_{\perp} \end{pmatrix} = \begin{pmatrix} a_{\parallel} e^{-i\delta_{\parallel}} \\ a_{\perp} e^{-i\delta_{\perp}} \end{pmatrix}, \tag{3.2}$$

with a the amplitude and δ the phase of a component. This is sufficient to describe any polarization of fully polarized light. If the phase difference $\Delta\delta = \delta_{\parallel} - \delta_{\perp} = 0$, the light is linearly polarized and the ratio of $a_{\parallel}$ and $a_{\perp}$ determines the polarization orientation. If $a_{\parallel} = a_{\perp}$ and $\Delta\delta = \pm\pi$, the light is circularly polarized. Any other combinations describe elliptical polarizations.

Optical media can change the polarization state of the light. To transfer this to the Jones-calculus means the medium transforms one vector into another and is therefore represented by a 2x2-matrix [4]. Then the new polarization state is

$$\mathbf{E}' = \mathbf{J} \cdot \mathbf{E} = \begin{bmatrix} J_{11} & J_{12} \\ J_{21} & J_{22} \end{bmatrix} \cdot \begin{pmatrix} E_{\parallel} \\ E_{\perp} \end{pmatrix}. \tag{3.3}$$

If light passes through n different optical media, the resulting Jones-matrix can be modeled by the multiplication $\mathbf{J}^{(n)} = \mathbf{J}_n \mathbf{J}_{n-1} ... \mathbf{J}_2 \mathbf{J}_1$, where $\mathbf{J}_1$ is the matrix of the first medium and $\mathbf{J}_n$ the matrix of the last [4].

3.2.2 Mueller-Stokes-calculus

Instead of using two complex-valued parameters, the polarization state of the light can also be described by four real-valued Stokes-parameters [1]

$$\begin{aligned} I &= E_{\parallel} E_{\parallel}^{*} + E_{\perp} E_{\perp}^{*} \\ Q &= E_{\parallel} E_{\parallel}^{*} - E_{\perp} E_{\perp}^{*} \\ U &= E_{\parallel} E_{\perp}^{*} + E_{\perp} E_{\parallel}^{*} \\ V &= i \left(E_{\parallel} E_{\perp}^{*} - E_{\perp} E_{\parallel}^{*} \right). \end{aligned} \tag{3.4}$$

I represents the total intensity in both, horizontally and vertically polarized light. Q and U represent the amount of linearly polarized light and V the amount of circularly polarized light. Often the parameters Q, U and V are also used as normalized parameters [1]. Then $Q/I = +1$ is horizontally polarized light, $Q/I = -1$ is vertically polarized light, $U/I = \pm 1$ is diagonally polarized light and $V/I = \pm 1$ is circularly polarized light. The Stokes-parameters have an advantage over the Jones-vectors: they can be used to describe partially polarized light with the degree of polarization (DOP) [1]

$$P = \sqrt{\frac{Q^2 + U^2 + V^2}{I^2}}\,. \tag{3.5}$$

Changes in DOP during propagation through a medium can be used to access how much it depolarizes the light.

Equivalently to the matrix multiplication in the Jones-calculus, changes in the polarization state in Mueller-Stokes-calculus can be expressed by the multiplication of the Mueller-matrix **M** with the stokes vector **S**.

$$\mathbf{S}' = \mathbf{M} \cdot \mathbf{S} = \begin{bmatrix} M_{11} & M_{12} & M_{13} & M_{14} \\ M_{21} & M_{22} & M_{23} & M_{24} \\ M_{31} & M_{32} & M_{33} & M_{34} \\ M_{41} & M_{42} & M_{43} & M_{44} \end{bmatrix} \begin{pmatrix} I \\ Q \\ U \\ V \end{pmatrix} \tag{3.6}$$

Jones-matrixes can be transformed to Mueller-Jones-matrixes via [5]

$$M_{kl} = \frac{1}{2}\,\mathrm{Tr}\left(\sigma_k \mathbf{J} \sigma_l \mathbf{J}^{\dagger}\right), \tag{3.7}$$

where σ_k and σ_l are the Pauli matrixes (k,l=0,1,2,3), Tr is the trace-operation and † indicates the transpose conjugate.

3.3 Implementation of polarization-sensitivity in OCT

3.3.1 Early PS-OCT

The first realization of a polarization-sensitive (PS) OCT system was based on bulk optics TD-OCT [6]. A schematic illustration is shown in Fig. 3.2. Linearly polarized light from a light source is split by BS and passing through QWPs in both sample (45° orientation) and reference (22.5° orientation) arm. It is split into orthogonal polarizations before detection by two PDs. The circular polarization in the sample arm is needed the be equally sensitive to all orientations of the optic axis of the sample. Each detector measures one polarization component [7, 8].

$$\mathbf{E}_{PD}(z) = \begin{pmatrix} E_H(z) \\ E_V(z) \end{pmatrix} = \begin{pmatrix} A_H(z) e^{i\phi_H(z)} \\ A_V(z) e^{i\phi_V(z)} \end{pmatrix} \tag{3.8}$$

It can be shown that the phase retardation can be calculated as [6, 7]

$$\eta(z) = \arctan\left(\frac{A_H(z)}{A_V(z)}\right) \tag{3.9}$$

and the optic axis orientation angle is with respect to the vertical polarization [8-10]

$$\theta_{OA} = \left(\pi + \phi_H(z) - \phi_V(z)\right)/2\,. \tag{3.10}$$

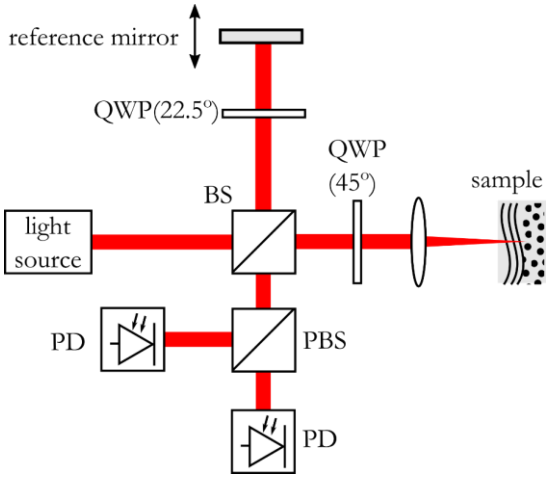

Fig. 3.2. Bulk-optics PS-OCT system based on TD-OCT. A low-coherent light course emits linearly polarized light which is split into sample and reference arm at the beam splitter (BS). It passes a quarter-wave plate (QWP) under 45° orientation in the sample arm which turns the linear into a circular polarization. In the reference arm it passes a QWP under 22.5° orientation. For detection the light is split into two orthogonal polarizations at the polarization beam splitter (PBS) and recorded with photodetectors (PD).

3.3.2 Fiber-based PS-OCT

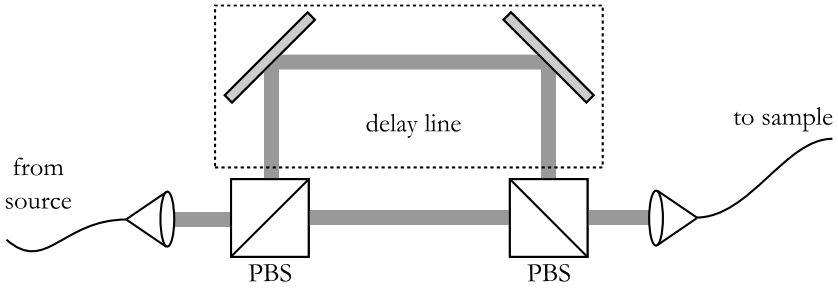

Fig. 3.3. Example for a polarization-delay-unit (PDU). Light is sent from a source through a single-mode fiber and transformed to a collimated beam in free space by a collimator. It is split into two orthogonal polarization states by the first PBS. One polarization state is traveling a longer optical path than the other. They are recombined at the second PBS and coupled into a single-mode fiber again which leads towards the sample.

Bulk-optics OCT systems have limited possibilities for *in vivo* applications and commercialization. Ensuring mechanical stability can be challenging and applications needing miniaturized flexible sample arms as are used e.g. for endoscopic applications [11] cannot be implemented with bulk-optics. Replacing bulk-optics with fiber-based systems increased significantly the number of possible applications [1]. Using optical fibers introduces other problems for PS-OCT because they show stress-induced birefringence [12]. Because of that the polarization state cannot be controlled in the way as shown in Fig. 3.2 where a circular

polarization state was incident on the sample. As a consequence, an optic-axis independent sensitivity for birefringence is not guaranteed anymore. This has been solved by the use of two orthogonal input polarizations in the sample arm in addition to the two polarization channels in the detection unit. This can be achieved by active components which modulate the polarization state [13-16] or passive components which split the polarization state into two states and send them to the sample with a time delay [17, 18]. The latter has also been used in the work of this thesis and is discussed here. An example for such a passive component is a polarization-delay unit (PDU) as shown in Fig. 3.3. Light is coupled from a single-mode fiber into free space. It is split into two polarization states at the first PBS. One state is delayed in time with respect to the other. Both are recombined at the second PBS and coupled into the single-mode fiber again to be sent towards the sample. The time delay creates a second image of the sample within the imaging depth of the OCT-system. Hence, this reduces the imaging depth by a factor of two.

System distortions due to fiber birefringence

Stress induced birefringence of the single-mode fibers poses a problem in the calculation of characteristic birefringent parameters for two reasons: 1. All birefringence which is measured in a sample is a mix of the birefringence of the OCT-device and the sample. 2. The birefringence of the fibers also changes when fibers are moved as the stress on the fibers changes. This requires algorithms which extract the birefringence parameters from only the sample and need only the data of an individual measurement and no additional calibration measurements. In Chapter 6 system distortions are corrected based on the Jones-matrix formalism. Therefore, this concept is described here but other implementations have been demonstrated, as well [11].

In a fiber-based system the measured depth-dependent polarization state $\mathbf{E}_{out}(z)$ can be modelled as [14]

$$\mathbf{E}_{out}(z) = \mathbf{J}_{out}\mathbf{J}_S(z)\mathbf{J}_{in}\mathbf{E}_{in}\,, \tag{3.11}$$

with the input polarization state $\mathbf{E}_{in}$, $\mathbf{J}_{in}$ the matrix describing the path from the point where two polarization states are created to the sample, $\mathbf{J}_S(z)$ the depth-dependent round-trip into the sample, scattering and backpropagation and $\mathbf{J}_{out}$ the path from the sample to the detector. A surface in the sample $\mathbf{E}_{surf}(z_{surf})$ (usually the first surface from which an interference can be measured) can be chosen for a correction. This way either $\mathbf{J}_{in}$ or $\mathbf{J}_{out}$ can be eliminated [14, 19].

$$\mathbf{E}_{out}(z)\mathbf{E}_{surf}(z_{surf})^{-1} = \mathbf{J}_{out}\mathbf{J}_S(z)\mathbf{J}_{out}{}^{-1} \tag{3.12}$$

The right side of Eq. (3.12) is a similar matrix to $\mathbf{J}_S$ and therefore contains the same eigenvalues as $\mathbf{J}_S$ which are used to calculate the phase retardation. Furthermore, the eigenvectors can be used to calculate the relative optic axis orientation. This is only the optic axis of the similar matrix but can contain useful information about the sample [19].

The birefringence of a fiber-based system is in general not uniform for all wavelengths.

This results that additional distortions remain after a correction such as discussed for Eq. (3.12). An example for that can be noticed in Eq. (3.1). The amount of phase retardation due to light propagation of a birefringent medium is dependent on the wavelength. A broad spectrum is used in OCT to achieve an axial resolution and therefore distortions will be present due to the wavelength-dependency of the birefringence. This effect is called polarization mode dispersion (PMD). The similar matrix of $\mathbf{J}_S$ can then be modelled as [20]

$$\mathbf{E}_{surf}{}^{-1}(k)\mathbf{E}_{out}(k) = \mathbf{J}_{in}{}^{-1}(k)\mathbf{J}_S(k)\mathbf{J}_{in}(k)\,. \tag{3.13}$$

Braaf *et al.* [20] have shown that through an analysis separating Eq. (3.13) into spectral bins, the PMD in the system can be analysed and compensated for. After PMD compensation, the left hand side of Eq. (3.13) can be written as

$$\mathbf{E}_{sample}(z) = \hat{\mathbf{E}}_{surf}{}^{-1}\hat{\mathbf{E}}_{out}(z) \tag{3.14}$$

with $\hat{\mathbf{E}}_{surf}{}^{-1}$ and $\hat{\mathbf{E}}_{out}(z)$ the measured surface and sample fields after PMD correction [20].

Calculation of birefringence parameters

In this paragraph parameters are described which can be used to characterize birefringence and are important for Chapter 6. It has been mentioned above that phase retardation can be calculated from eigenvalues of $\mathbf{E}_{sample}$. This represents the retardation when light travels twice through the tissue and is scattered/reflected in between. For further purposes it is called cumulative double-pass phase retardation (DPPR) [20]

$$\eta_{DPPR} = \left|\arg\left(\lambda_1\lambda_2^{*}\right)\right|, \tag{3.15}$$

with λ_1 and λ_2 the eigenvalues of $\mathbf{E}_{sample}$.

When DPPR is calculated for a whole B-scan, each pixel represents the phase retardation that the light has collected from tissue before it. For more intuitive interpretations and quantitative analyses, a parameter is of interest which is proportional to the local distribution of birefringent tissue. A calculation of such a parameter based on differential Mueller-matirces has been reported earlier [21] and is also used in this thesis. First, $\mathbf{E}_{sample}$ is converted into a Mueller-Jones-matrix according to Eq. (3.7) and further into a Mueller-matrix $\mathbf{M(z)}$ by spatial averaging. As second step the local Mueller-matrix can be calculated over a small depth displacement δz as

$$\Delta\mathbf{M} = \mathbf{M}(z+\delta z)\mathbf{M}^{-1}(z) \tag{3.16}$$

and the differential Mueller-matrix through the matrix logarithm

$$\mathbf{m} = \log\ \mathrm{m}(\Delta\mathbf{M})\,. \tag{3.17}$$

Elements of **m** can be used to calculate the relative optic axis and phase retardation as a vector [21, 22]

$$\mathbf{\Gamma} = \frac{1}{2}\begin{pmatrix} m_{34} - m_{43} \\ m_{24} - m_{42} \\ m_{32} - m_{23} \end{pmatrix}. \tag{3.18}$$

If phase retardation is extracted from Eq. (3.18) as $\gamma = \|\mathbf{\Gamma}\|$ it is called local birefringence to avoid confusion with DPPR. It is related to the refractive index difference as $\Delta n = \gamma/(k_c 2\delta z)$ with k_c the central wavenumber [21].

As an additional contrast mechanism to identify birefringent structures the optic axis uniformity (OAxU) was used due to its ability to localize structures axially and its superior contrast-to-noise ratio in comparison to local birefringence [23]. First, normalized optic axis elements are calculated $(H, N, M)^T = \mathbf{\Gamma}/\gamma$. Then, the elements are averaged spatially to deliver H_{avg}, N_{avg} and M_{avg}. Finally, the OAxU is calculated as [23]

$$\mathrm{OAxU} = \sqrt{{H_{avg}}^2 + {N_{avg}}^2 + {M_{avg}}^2}\,. \tag{3.19}$$

The interested reader is referred to [23].

References

1. B. H. Park and J. F. de Boer, "Polarization Sensitive Optical Coherence Tomography," in *Optical Coherence Tomography: Technology and Applications*, W. Drexler and J. G. Fujimoto, eds. (Springer International Publishing, Cham, 2015), pp. 1055-1101.
2. X. R. Huang, "Polarization properties of the retinal nerve fiber layer," Bull Soc Belge Ophtalmol, 71-88 (2006).
3. J. M. Bennett, "Polarization," in *Handbook of Optics,* 2 ed., M. Bass, ed. (McGraw-Hill, Inc., 1995), pp. 5.1-5.20.
4. R. C. Jones, "A new calculus for the treatment of optical systems I. Description and discussion of the calculus," J Opt Soc Am **31**, 488-493 (1941).
5. R. Barakat, "Bilinear constraints between elements of the 4 x 4 Mueller-Jones transfer matrix of polarization theory," Opt Commun **38**, 159-161 (1981).
6. M. R. Hee, D. Huang, E. A. Swanson, and J. G. Fujimoto, "Polarization-Sensitive Low-Coherence Reflectometer for Birefringence Characterization and Ranging," J Opt Soc Am B **9**, 903-908 (1992).
7. J. F. de Boer and T. E. Milner, "Review of polarization sensitive optical coherence tomography and Stokes vector determination," J Biomed Opt **7**, 359-371 (2002).
8. C. K. Hitzenberger, E. Götzinger, M. Sticker, M. Pircher, and A. F. Fercher, "Measurement and imaging of birefringence and optic axis orientation by phase resolved polarization sensitive optical coherence tomography," Opt Express **9**, 780-790 (2001).
9. J. F. de Boer, T. E. Milner, M. J. van Gemert, and J. S. Nelson, "Two-dimensional birefringence imaging in biological tissue by polarization-sensitive optical coherence tomography," Opt Lett **22**, 934-936 (1997).
10. J. F. de Boer, T. E. Milner, and J. S. Nelson, "Determination of the depth-resolved Stokes parameters of light backscattered from turbid media by use of polarization-sensitive optical coherence tomography," Opt Lett **24**, 300-302 (1999).
11. J. F. de Boer, C. K. Hitzenberger, and Y. Yasuno, "Polarization sensitive optical coherence tomography - a review [Invited]," Biomed Opt Express **8**, 1838-1873 (2017).
12. G. P. Agrawal, "Optical Fibers," in *Fiber-Optic Communication Systems,* 3 ed. (Wiley Interscience, 2002), pp. 23-76.
13. C. E. Saxer, J. F. de Boer, B. H. Park, Y. Zhao, Z. Chen, and J. S. Nelson, "High-speed fiber based polarization-sensitive optical coherence tomography of in vivo human skin," Opt Lett **25**, 1355-1357 (2000).
14. B. H. Park, M. C. Pierce, B. Cense, and J. F. de Boer, "Jones matrix analysis for a polarization-sensitive optical coherence tomography system using fiber-optic components," Opt Lett **29**, 2512-2514 (2004).
15. B. H. Park, M. C. Pierce, B. Cense, S. H. Yun, M. Mujat, G. J. Tearney, B. E. Bouma, and J. F. de Boer, "Real-time fiber-based multi-functional spectral-domain optical coherence tomography at 1.3 mu m," Opt Express **13**, 3931-3944 (2005).
16. B. Cense, M. Mujat, T. C. Chen, B. H. Park, and J. F. de Boer, "Polarization-sensitive spectral-domain optical coherence tomography using a single line scan camera," Opt Express **15**, 2421-2431 (2007).
17. Y. Lim, Y. J. Hong, L. Duan, M. Yamanari, and Y. Yasuno, "Passive component based multifunctional Jones matrix swept source optical coherence tomography for Doppler and polarization imaging," Opt Lett **37**, 1958-1960 (2012).
18. B. Baumann, W. Choi, B. Potsaid, D. Huang, J. S. Duker, and J. G. Fujimoto,

"Swept source/Fourier domain polarization sensitive optical coherence tomography with a passive polarization delay unit," Opt Express **20**(2012).
19. Y. Yasuno, M.-J. Ju, Y. J. Hong, S. Makita, Y. Lim, and M. Yamanari, "Jones Matrix Based Polarization Sensitive Optical Coherence Tomography," in *Optical Coherence Tomography: Technology and Applications*, W. Drexler and J. G. Fujimoto, eds. (Springer International Publishing, Cham, 2015), pp. 1137-1162.
20. B. Braaf, K. A. Vermeer, M. de Groot, K. V. Vienola, and J. F. de Boer, "Fiber-based polarization-sensitive OCT of the human retina with correction of system polarization distortions," Biomed Opt Express **5**, 2736-2758 (2014).
21. M. Villiger, D. Lorenser, R. A. McLaughlin, B. C. Quirk, R. W. Kirk, B. E. Bouma, and D. D. Sampson, "Deep tissue volume imaging of birefringence through fibre-optic needle probes for the delineation of breast tumour," Sci Rep-Uk **6**(2016).
22. R. M. A. Azzam, "Propagation of Partially Polarized-Light through Anisotropic Media with or without Depolarization - Differential 4x4 Matrix Calculus," J Opt Soc Am **68**, 1756-1767 (1978).
23. J. Willemse, M. G. O. Gräfe, J. A. van de Kreeke, F. Feroldi, F. D. Verbraak, and J. F. de Boer, "Optic axis uniformity as a metric to improve the contrast of birefringent structures and analyze the retinal nerve fiber layer in polarization-sensitive optical coherence tomography," Opt Lett **44**, 3893-3896 (2019).